Surfaces and Interfaces 73 (2025) 107622

Contents lists available at ScienceDirect

Surfaces and Interfaces

journal homepage: www.sciencedirect.com/journal/surfaces-and-interfaces

High-affinity capture of recombinant streptococcal protein G and Its application in serum proteomics with immunoglobulin G-coated magnetic nanoparticles

Dajun Zhang [a,1], Yufei Ma [a,1], Ying Wang [a], Xiangyu Liu [a], Mengfan Zhao [a], Yuanke Wang [c], Song Gao [c], Fu Ren [b,*], Qing Chen [a,b,*]

[a] School of Pharmacy, Shenyang Medical College, Shenyang 110034, China
[b] Shenyang Key Laboratory for Phenomics, Liaoning Province Key Laboratory for Phenomics of Human Ethnic Specificity and Critical Illness, Shenyang Medical College, Shenyang 110034, China
[c] Central Hospital of Shenyang Sujiatun, Shenyang 110101, China

ARTICLE INFO

Keywords:
Magnetic nanoparticles
Recombinant proteins
Solid-phase capture
Serum proteomics

ABSTRACT

A new solid-phase extraction agent, IgG@ Fe_3O_4-PEI, was successfully developed by conjugating immunoglobulin G (IgG) with amino-functionalized magnetic nanoparticles (Fe_3O_4-PEI). The IgG@Fe_3O_4-PEI composite was characterized using various techniques including infrared spectroscopy, Raman spectroscopy, magnetic property testing, Zeta potential measurements, energy spectrum analysis, scanning electron microscopy (SEM), and transmission electron microscopy (TEM). Because of the presence of a specific binding domain in the Fc fragment of IgG, the IgG@Fe_3O_4-PEI composite demonstrated highly selective adsorption of recombinant streptococcal G protein (rSPG) under optimal experimental conditions. At pH 6.0, the IgG@Fe_3O_4-PEI composite (0.5 mg) achieved a maximum adsorption efficiency of 93.96 % for rSPG at a concentration of 100 μg mL^{-1}. Adsorption model simulations indicated that the adsorption behavior followed the *Langmuir* adsorption model, with a theoretical maximum adsorption capacity of 125.0 mg g^{-1}. The enriched rSPG was eluted and recovered using Britton-Robinson (BR) buffer at pH 10.0, achieving a recovery efficiency of 95.8 %. In practical applications, the IgG@Fe_3O_4-PEI magnetic nanoparticles effectively enriched rSPG from an *Escherichia coli* expression system, and SDS-PAGE analysis confirmed the successful isolation of highly pure rSPG. Furthermore, the IgG@Fe_3O_4-PEI magnetic nanoparticles were used to capture proteins from human serum samples. After enrichment and processing, 430 proteins were identified, including 34 that were undetectable in untreated serum samples. This validated the high sensitivity and specificity of this method in serum proteomics, demonstrating its potential for isolating and identifying low-abundance proteins in complex biological samples. The developed system offers a valuable tool for advancing human serum proteomics research and targeted protein analysis.

1. Introduction

Recombinant proteins play a crucial role in treating a range of diseases, including infectious diseases and cancer, which remain major global causes of mortality [1]. Biotechnological advancements are continuously enhancing the diversity and efficacy of these therapeutic proteins, providing new treatment opportunities. Currently, a wide range of recombinant proteins, such as antibodies, vaccines, and enzymes are used as drugs [2]. Streptococcal protein G (SPG) initially derived from streptococcal bacteria, is now widely produced through recombinant DNA technology in expression hosts like *E. coli* to fulfill the increasing demands of scientific research [3]. As a high-affinity protein, rSPG is widely used in experimental techniques such as immunoprecipitation and Western blotting. For example, in immunoprecipitation, specific antibodies targeting the protein of interest can bind to protein A/G affinity beads, enabling the identification of interacting molecules [4]. rSPG is also employed as a diagnostic tool for antibody detection, contributing to disease identification and the assessment of therapeutic responses. For example, in slide agglutination assays employing purified protein derivative (PPD) antigens, rSPG enhances the sensitivity of

* Corresponding authors.
E-mail addresses: rf@symc.edu.cn (F. Ren), chenqing0906@symc.edu.cn (Q. Chen).
[1] Dajun Zhang and Yufei Ma contributed equally to this work.

https://doi.org/10.1016/j.surfin.2025.107622
Received 22 October 2024; Received in revised form 21 August 2025; Accepted 4 September 2025
Available online 5 September 2025

detecting bovine tuberculosis (BTB) antibodies in serum samples [5]. Furthermore, rSPG contains multiple domains that serve as versatile tags [6]. For instance, Z-domain peptides, derived from the double-limited domain of protein G, are employed to precisely position antibodies in sensitive immunoassays and biosensors [7].

Beyond its established laboratory applications, rSPG specifically binds to the Fc fragment of immunoglobulin G (IgG), a property that plays a crucial role in various biological processes [8]. The Fc region of IgG interacts with various Fc-binding proteins present in the bloodstream, contributing to immune response modulation, immune regulation, as well as pathogen defense [9,10]. These proteins include Fc receptors (e.g., FcγRI, FcγRII, FcγRIII) [11], complement components like C1q [12], and various Fc-binding proteins, including SPG and those secreted by pathogens [13]. These Fc-binding proteins contribute to immune clearance, immune modulation, and the defense against pathogens, highlighting their significance in immune system function [14]. Therefore, understanding the interactions between rSPG and the Fc fragment provides valuable insights into immune-related diseases and potential therapeutic strategies [15].

Solid-phase capture is a widely used technique in biological and chemical research for isolating and purifying specific molecules, including proteins, nucleic acids, or other biologically functional units, from complex mixtures [16,17]. The method relies on the affinity of the target molecule for a solid-phase material, which may be coated with specific ligands such as immunosorbents, aptamer-modified surface [18], or a phage display peptide [19]. Yang et al. engineered filamentous phages through genetic and chemical modifications to develop an affinity interface with enhanced specificity and resistance to non-specific binding. This approach enabled the selective capture and identification of circulating tumor cells based on the unique interactions of phage fibers [19]. Increasing research evidence highlights that molecular capture technology significantly improves the specificity of solid-phase extraction, thus enabling the isolation of highly purified target compounds [20,21]. Currently, the most extensively studied solid-phase extraction materials include carbon-based materials such as graphene [22], molecularly imprinted polymers [23], magnetic nanoparticles [24], metal-organic frameworks [25], and covalent organic frameworks [26]. Various solid-phase materials are tailored to specific analytical targets and sample types, ensuring optimal selectivity and efficiency in extraction processes.

Therefore, in practical applications, appropriate solid-phase support materials are selected based on specific circumstances. This technology is widely used in protein isolation, purification, and large-scale production of recombinant proteins. For example, a novel composite material, TeW_6@ZIF-8, can be synthesized by integrating polyoxometalate TeW_6 with the metal-organic framework ZIF-8. This composite material demonstrated exceptional adsorption capacity for cytochrome C and has been effectively employed for its separation and purification from pig heart protein extracts [27]. Mengmeng Wang et al. developed a tetra-nickel-substituted polyoxotungstate for the separation of HIS6-labeled proteins from cell lysates, demonstrating higher efficiency compared to the commercial NTA-Ni^{2+} column [28].

Fe_3O_4 magnetic nanoparticles are nanoscale particles with remarkable magnetic properties, biocompatibility, and precisely controllable sizes [28]. These characteristics make them highly versatile for applications in biomedicine and solid-phase extraction [29,30]. In biomedicine, Fe_3O_4 magnetic nanoparticles hold significant potential for tumor therapy and diagnostics, serving as drug delivery carriers and contrast agents for magnetic resonance imaging [31]. For example, Shen et al. designed and synthesized platinum-loaded Fe_3O_4 magnetic nanoparticles functionalized with lactoferrin (LF) and RGD dimer (RGD_2) to enhance ferroptosis therapy (FT) for orthotopic brain tumors. These nanoparticles can cross the blood-brain barrier and are taken up by cancer cells, where they release iron ions and platinum. This process enhanced the Fenton reaction, generating reactive oxygen species that trigger cancer cell death. Magnetic nanoparticles also enable magnetic resonance imaging (MRI) for real-time monitoring of tumor responses to ferroptosis therapy [32]. In solid-phase extraction, Fe_3O_4 magnetic nanoparticles are widely employed for the enrichment and separation of target compounds, including organic pollutants and heavy metal ions in water samples [33,34]. Fe_3O_4 magnetic nanoparticles are also effective in protein separation and purification. For example, Fe_3O_4/Au nanoparticles modified with 2-mercaptobenzimidazole sulfonic acid (MBISA) (Fe_3O_4/Au-MBISA) enable the rapid, efficient, and selective extraction of lysozyme from egg white. The maximum adsorption capacity of lysozyme onto Fe_3O_4/Au-MBISA was determined to be 346 μg mg^{-1}. After seven cycles of adsorption and desorption, they retain about 91 % of their initial adsorption capacity, demonstrating their high reusability and stability [35]. In summary, Fe_3O_4 magnetic nanoparticles, with their strong magnetic responsiveness, high sensitivity, outstanding selectivity, and ease of application, represent an ideal material for solid-phase extraction, offering promising new possibilities for the efficient and rapid separation and purification of proteins.

In this study, IgG was immobilized on the surface of Fe_3O_4 magnetic nanoparticles modified with polyethyleneimine (PEI), resulting in the successful development of a novel bioconjugated magnetic nanoparticle (IgG@Fe_3O_4-PEI). The composite, demonstrating selective adsorption properties for rSPG due to the specific binding interaction between IgG and rSPG, effectively separated and purified rSPG from *E. coli* expression systems. This achievement not only broadens the application potential of Fe_3O_4 magnetic nanoparticles in protein separation and purification but also expands their scope in life sciences. Furthermore, the IgG@Fe_3O_4-PEI composite was applied in the pretreatment of serum samples, providing a valuable tool for proteomics research and offering key insights for protein analysis in complex biological samples.

2. Experimental section

2.1. Materials and reagents

rSPG was obtained from Beyotime Biotechnology (Shanghai, China). IgG, bovine serum albumin (BSA), and lysozyme (Lys) were purchased from Sigma Aldrich (St. Louis, USA). Hyperbranched polyethyleneimine (PEI, E107079, M.W. = 10,000 Da, branching degree = 0.3 ± 0.05, viscosity (25 °C, neat) = 40,000–150,000 cP, form = colorless viscous/liquid) was procured from Shanghai Aladdin Biochemical Technology Co., LTD (Shanghai, China). $FeCl_3$•$6H_2O$ was purchased from Adamasbeta (Shanghai) Chemical Reagent Co., LTD (Shanghai, China). Other reagents, including ethylene glycol, ethylene glycol, anhydrous ethanol, N, imidazole, trimethylol aminomethane (Tris), sodium dodecyl sulfate (SDS), Coomassie bright blue (G250, R250), glycine, methylene bisacrylamide, ammonium persulfate were obtained from Sinopath Chemical Reagent Co., LTD (Shanghai, China). The water used in the experiments was secondary deionized water (ddH_2O, 18 MΩ·cm).

2.2. Instrumentation

The FT-IR spectra were recorded using a Nicolet 6700 instrument (Thermo Fisher Nicolet, USA) with wavenumbers ranging from 400 to 4000 cm^{-1}. Raman spectra were acquired using a Renishaw inVia Raman spectrometer (Renishaw, UK). SEM images were captured using a Hitachi SU8020 scanning electron microscope (Hitachi, Japan), and energy X-ray dispersive (EDS) analysis was performed using a HORIBA EX350 instrument (HORIBA Scientific, Ltd., France). TEM images were recorded using HITACHI H7650 transmission electron microscope (Hitachi, Japan). Magnetic properties were determined using a Vibrating Sample Magnetometer Model 8604 (Lake Shore, USA). Circular dichroism spectra and absorbance measurements were recorded using a MOS-450 automatic transcription spectropolarimeter (Bio-Logic, France) at 293 K and a U-3900 UV–VIS spectrophotometer (Hitachi, Japan), respectively. An STA 449 F3/F5 (NETZSCH, Germany) was used for thermal analysis. A Bruker timsTOF HT mass spectrometer (Bruker

Corporation, USA) was used for mass spectrometry. Liquid chromatography was performed using an EASY-nLC 1200 system (Thermo Fisher, USA).

2.3. Synthesis of the IgG@Fe_3O_4-PEI composite

Fe_3O_4-PEI magnetic nanoparticles were synthesized using PEI as a stabilizer through a solvothermal method. A mixture of 0.135 g $FeCl_3$•$6H_2O$ (yellow color) and 1.8 g sodium acetate was dissolved in 20 mL glycol. Add 0.5 g colorless hyperbranched polyethylenimide viscous by drip and stir continuously at room temperature for 45 min to form a yellow colloidal mixture. Transfer the mixture to a teflon sealed stainless steel autoclave with a capacity of 50 mL. Set the oven temperature to 200 °C and place the autoclave in the oven for 12 h. Then it was cooled to room temperature, the resulting products were separated by magnetic separation and washed twice with anhydrous ethanol and twice with distilled water. The black Fe_3O_4-PEI powder was obtained by drying at 60 °C for 12 h [36].

A total of 5.0 mg of IgG was precisely measured and placed in a centrifuge tube followed by the addition of 5.0 mL of ddH_2O, resulting in a 1.0 mg/mL IgG solution, which was then stored in a refrigerator for future use. Meanwhile, 4.0 mg of Fe_3O_4-PEI magnetic nanoparticles were mixed with 1.0 mL of IgG (1.0 mg/ml) protein solution and allowed to shake for 45 min. The IgG@Fe_3O_4-PEI product was collected using a magnetic field, washed three times with water, and then freeze-dried.

2.4. Adsorption/desorption of proteins by the IgG@Fe_3O_4-PEI composite

The adsorption behavior of IgG@Fe_3O_4-PEI on rSPG, BSA, and Lys at different pH conditions was studied using BR buffers with varying pH of 4.0–10.0. In this process, 0.5 mg of IgG@Fe_3O_4-PEI composite was added to a centrifuge tube, followed by 100 μL of a 100 μg/mL protein solution and shaken for 60 min to promote adsorption. Afterward, the composite was separated from the solution using a magnetic field. The supernatant (60 μL) was then mixed with 300 μL of Coomassie Brilliant Blue G250 solution, and the absorbance was measured at 595 nm using a UV spectrophotometer to calculate the residual protein concentration in the solution. A standard working curve was used to calculate the protein concentration before and after adsorption.

After the adsorption process, the IgG@Fe_3O_4-PEI composite was collected, and to improve protein recovery, 200 μL of BR buffer (pH 10.0) was added. The mixture was then shaken for 30 min, followed by separation under a magnetic field. The supernatant was then collected for desorption efficiency evaluation or stored for further research.

2.5. Separation of rSPG from protein mixture samples

The IgG@Fe_3O_4-PEI composite (0.5 mg) was mixed with 100 μL of a protein solution containing 100 μg·mL^{-1} rSPG and Lys at pH 6.0). The mixture was thoroughly shaken for 60 min, followed by magnetic separation to collect the supernatant. To recover the adsorbed proteins, BR buffer (pH 10.0) was added as the elution buffer, and the proteins in both the supernatant and elution buffer were then analyzed using sodium dodecyl sulfate-polyacrylamide gel electrophoresis (SDS-PAGE) [37].

2.6. Separation of rSPG from complex biological samples

E. coli BL21 (DE3) was transformed with the positive recombinant plasmid pET-21a(+)-rSPG and a single colony was selected for inoculation into LB medium containing 100 mg/mL ampicillin sodium. The culture was shaken overnight, and then 300 μL was transferred into 10 mL of fresh LB medium with ampicillin sodium, followed by incubation at 37 °C and 160 rpm for 120–150 min until the OD_{600} value reached 0.6–0.8. Then, 150 μL of IPTG (final concentration 1 mmol L^{-1}) was added to induce protein expression, and the culture was incubated at 37 °C for approximately 5 h. After incubation, the culture was centrifuged at 10,000 rpm for 3 min to collect the bacterial pellet. The pellet was washed multiple times with PBS buffer, subjected to freeze-thaw cycles to disrupt the cells, resuspended in BR buffer (pH 6.0), and sonicated for further cell disruption. The mixture was then centrifuged at 7,000 rpm and 4 °C for 15 min to remove the precipitate, resulting in a clear bacterial lysate, which was stored at −20 °C for future use.

IgG@Fe_3O_4-PEI composite (0.5 mg) was added to a 0.5-mL centrifuge tube, followed by the addition of 100 μL of bacterial lysate. The mixture was shaken vigorously for 60 min, and the supernatant after adsorption was collected using magnetic separation. The protein-bound composite was washed with ddH_2O to remove any non-target proteins that remained on the material surface. BR buffer (pH 10.0) was then used as the elution solution to recover the target protein adsorbed onto the material. Finally, the supernatant and elution solution were analyzed using SDS-PAGE.

2.7. Extraction of low-abundance proteins from serum samples

Human blood serum samples were diluted 500-fold with BR buffer (pH 6.0) to reduce viscosity and enhance interaction with the composite. Following this, 0.5 mg of the IgG@Fe_3O_4-PEI composite was added to 500 μL of the diluted serum solution, and the mixture was vigorously agitated for 60 min to ensure efficient binding of serum proteins to the composite. After the binding step, magnetic separation was performed to isolate the composite-bound proteins, and the supernatant was subsequently collected for further analysis. High-resolution mass spectrometry was used to detect low-abundance proteins in the eluate. The acquired mass spectra were then analyzed using protein databases such as UniProt or Swiss-Prot, enabling the identification and detailed characterization of proteins in the serum sample.

3. Results and discussion

3.1. Characterization of the IgG@Fe_3O_4-PEI composite

Fe_3O_4-PEI was synthesized using the solvothermal approach, with polyethyleneimine (PEI) acting as a stabilizer to prevent particle aggregation while introducing a high density of surface amino (-NH_2) groups on the magnetic nanoparticles. In the solvothermal synthesis system, polyethyleneimine (PEI) provides colloidal stability to Fe_3O_4 nanoparticles via two complementary mechanisms: (i) steric stabilization through polymeric chain wrapping that creates physical separation between particles, and (ii) electrostatic stabilization mediated by surface-bound protonated amine groups (-NH^{2+}) that establish interparticle repulsive forces [38]. IgG binds to Fe_3O_4 -PEI via electrostatic interactions, enabling effective functionalization. The Zeta potential data (Fig. 1D) indicated that Fe_3O_4-PEI had a negative surface charge at pH 6.0, while IgG (pI 8.0) was positively charged under the same conditions. Therefore, under specific conditions, IgG can be immobilized on the Fe_3O_4-PEI surface via electrostatic interactions, particularly in laboratory ddH_2O at pH ≈ 6.0) (Scheme 1).

Fig. 1A shows the FT-IR spectra of the Fe_3O_4-PEI and IgG@Fe_3O_4-PEI composites. In the FT-IR spectrum of Fe_3O_4-PEI, the absorption peak at 585 cm^{-1} corresponded to Fe-O vibrations [39], whereas the absorption peaks at 1640 cm^{-1} and 3440 cm^{-1} were attributed to the primary amine groups ((R-NH_2), confirming the successful PEI coating on Fe_3O_4 magnetic nanoparticles [40]. In the infrared spectrum of the IgG@Fe_3O_4-PEI composite, alongside the characteristic peaks of Fe_3O_4-PEI, new absorption bands appeared at 1230 and 1510 cm^{-1}, corresponding to the C—O and *C = O* bonds of the amide group, respectively [41]. The infrared spectroscopy further confirmed the successful synthesis of the IgG@Fe_3O_4-PEI composite.

Fig. 1B shows the Raman spectra of the Fe_3O_4-PEI and IgG@Fe_3O_4-PEI composites. In the Raman spectrum of Fe_3O_4-PEI, the characteristic

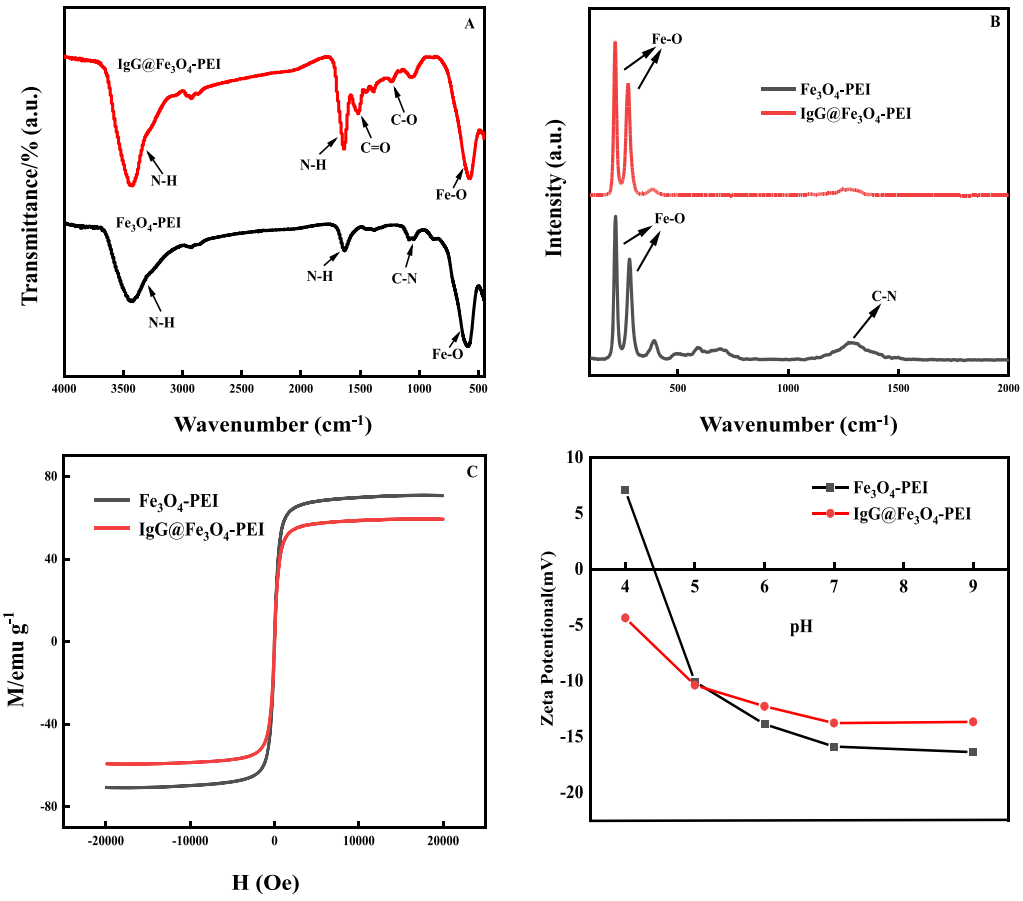

Fig. 1. FT-IR spectra of the Fe_3O_4-PEI and IgG@Fe_3O_4-PEI composites (A). Raman spectra of the Fe_3O_4-PEI and IgG@Fe_3O_4-PEI composites (B). VSM curves of Fe_3O_4-PEI and IgG@Fe_3O_4-PEI (C). Zeta potential of Fe_3O_4-PEI and IgG@Fe_3O_4-PEI (D).

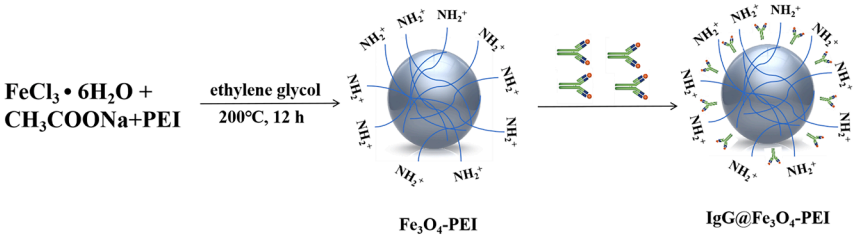

Scheme 1. Preparation of IgG@Fe_3O_4-PEI.

peaks of Fe-O appeared at 217 and 279 cm^{-1} [42] whereas the peak observed at 589 cm^{-1} corresponded to the lattice vibration mode of Fe_3O_4-PEI. The peak at 1274 cm^{-1} attributed to the C—N stretching vibration of PEI [43] confirmed the successful coating of PEI on the Fe_3O_4 surface. In the Raman spectrum of the IgG@Fe_3O_4-PEI composite, the lattice vibration mode disappeared due to structural changes induced by IgG modification. The observed alteration disrupted the original lattice vibration, leading to its disappearance. Furthermore, the C—N stretching vibration at 1275 cm^{-1} weakened, likely because IgG modification masked the PEI-associated C—N signal, affecting the elastic scattering of light on the sample surface. These findings confirmed the successful modification of Fe_3O_4-PEI by IgG.

Fig. 1C presents the hysteresis loops of Fe_3O_4-PEI and IgG@ Fe_3O_4-PEI composites at room temperature, showing saturation magnetization values of 70.85 and 59.41 emu g^{-1}, respectively. The slight decrease in magnetization confirmed the successful attachment of IgG to Fe_3O_4-PEI while preserving the composite's superparamagnetic properties.

Fig. 1D illustrates the Zeta potential variations of Fe_3O_4-PEI and IgG@ Fe_3O_4-PEI composites across different pH levels. Fe_3O_4-PEI demonstrated a negative Zeta potential above pH 4.5 and a positive potential below this threshold. Therefore, the isoelectric point of Fe_3O_4-PEI was determined to be approximately 4.5. Following IgG modification through electrostatic interactions, the Zeta potential of IgG@ Fe_3O_4-PEI remained negative across all pH values, confirming that the composite surface acquired a net negative charge after IgG attachment. Meanwhile, EDS was used to determine the elemental composition of the composite. The atomic percentages of C, N, O, and Fe in the composite were determined to be 47.05, 11.52, 23.28, and 18.15 %, respectively.

Fig. 2A shows that the synthesized Fe_3O_4-PEI is composed of many small particles aggregated into larger clusters, with a size of approximately 100 nm. This aggregation can be attributed to the presence of PEI, a high-molecular-weight polymer, which promotes the linking of individual particles to form larger structures. Fig. 2B shows that IgG modification increases the size of the nanoparticles to around 200 nm,

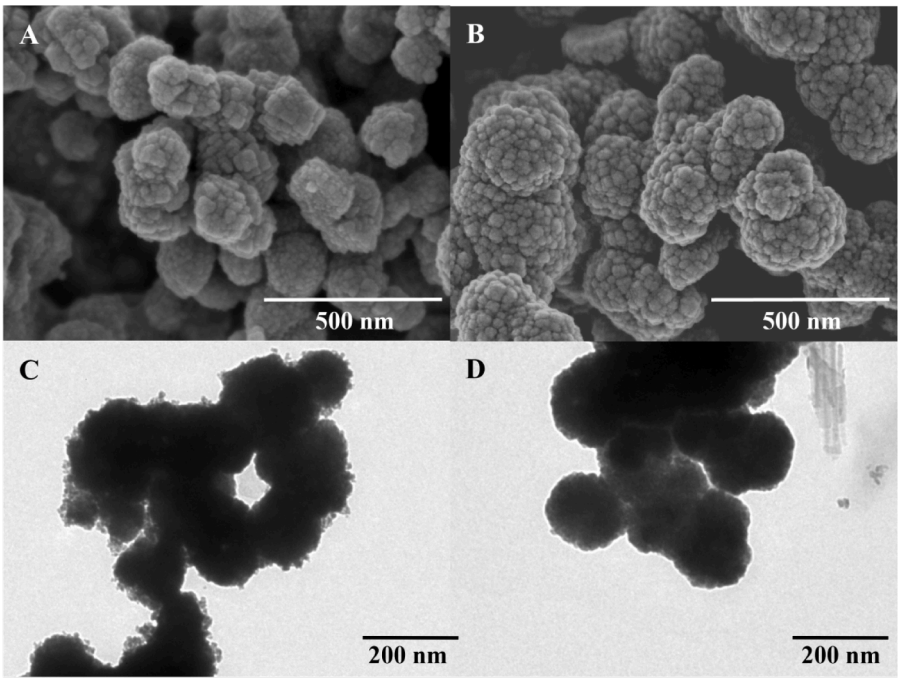

Fig. 2. SEM (A, B) and TEM images of Fe_3O_4-PEI and IgG@Fe_3O_4-PEI composite (C, D).

resulting in uniform and smooth aggregation. Fig. 2C and 2D are TEM images of Fe_3O_4-PEI and IgG@Fe_3O_4-PEI, respectively. In Fig. 2C, Fe_3O_4-PEI mainly presents as magnetic spheres adhering to each other, forming larger particles. In Fig. 2D, due to the modification of IgG, the edges of the magnetic nanoparticles become smooth and uniform, and the aggregation becomes tighter.

3.2. Adsorption of proteins by the IgG@Fe_3O_4-PEI composite

In this experiment, the adsorption capacity of the IgG@Fe_3O_4-PEI composite on three model proteins (rSPG, BSA, and Lys) was studied. The adsorption of the three proteins on IgG@Fe_3O_4-PEI was examined across pH 4.0–10.0. As shown in Fig. 3A, three proteins with different isoelectric points including rSPG, BSA, and Lys were adsorbed onto the composite material under varying pH conditions. The results demonstrated that the magnetic sphere material selectively adsorbed rSPG, while the adsorption efficiency for BSA and Lys was minimal. Moreover, optimization studies revealed that the material exhibited the highest adsorption efficiency for rSPG at pH 6.0, providing a basis for further condition refinement. The adsorption efficiency of rSPG increased progressively, reaching a maximum of 93.96 % at pH 6.0 before sharply decreasing. rSPG has three IgG binding domains that can bind to Fc fragments of IgG. The IgG binding domain of rSPG consists of four beta chains surrounded by a central α-helix segment. Among them, amino acid residues on the α-helix can maintain a stable binding state with IgG Fc fragments, participating in the formation of most stable hydrogen bonds. At the same time, rSPG also has two hydrophobic amino acid residues (ALA23 and ALA24), which can interact with hydrophobic amino acid residues of IgG Fc fragments (MET-252, ILE-253, etc.) to form hydrophobic bonds.The selective adsorption of rSPG by IgG@Fe_3O_4-PEI was primarily attributed to hydrogen bonding between the Fc fragment of IgG and the immunoglobulin-binding region of rSPG [44,45]. At pH 6.0 near the pI of rSPG (4.79), its hydrophobicity increased, allowing interaction with the IgG@Fe_3O_4-PEI composite through hydrogen bonding. The negative charges of amino acid residues (e.g., glutamic acid, aspartate) and sugar groups on IgG molecules are the most stable in electrolyte solutions and are not excessively deprotonated. As a result, IgG maintains its negatively charged state at pH 6,

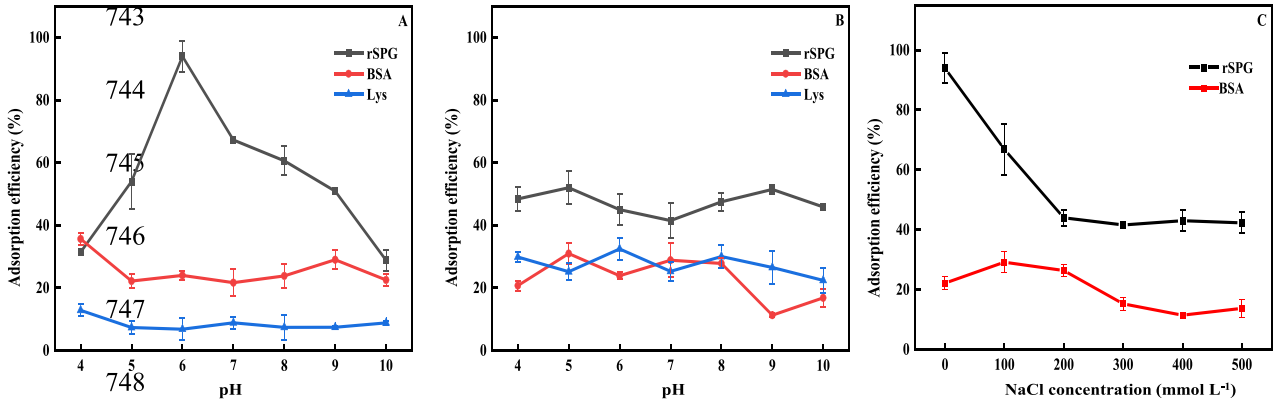

Fig. 3. pH-dependent adsorption behaviors of rSPG, BSA, and Lys onto IgG@Fe_3O_4-PEI composite surface (A) and Fe_3O_4-PEI surface (B). Effect of ionic strength on the adsorption efficiency of rSPG, BSA, and Lys (C). Protein solution: 100 μg mL^{-1}, 100 μL; IgG@Fe_3O_4-PEI: 0.5 mg.

resulting in strong electrostatic adsorption with positively charged surfaces, such as the positively charged amino region of rSPG.Under acidic conditions, the proton (H^+) content in the solution leads to the protonation of hydrogen bond donors or acceptors, weakening the stability and strength of hydrogen bonds [46]. Therefore, at pH < 6.0, the adsorption efficiency of the IgG@Fe_3O_4-PEI composite for rSPG decreased. Fig. 1D shows that the composite carried a negative charge. As pH increases, the charge distribution of IgG changes. At pH values greater than 6, some amino acids (e.g., lysine, arginine, etc.) on IgG may be deprotonated, resulting in an increase in certain positively charged areas on the IgG surface. This causes IgG to have a neutral or positively charged overall charge at pH > 6, whereas rSPG usually has a negative charge in neutral or slightly acidic environments. As a result, the electrostatic attraction between IgG and rSPG is weakened, resulting in a lower adsorption efficiency. However, at pH 6.0, the IgG@Fe_3O_4-PEI composite showed minimal adsorption of BSA and Lys, making pH 6.0 the optimal condition for the selective separation and purification of rSPG.

The study also evaluated the influence of unmodified Fe_3O_4-PEI on protein adsorption efficiency across varying pH levels. As shown in Fig. 3B, the adsorption efficiency of Fe_3O_4-PEI on rSPG was approximately 40–50 %, much lower than the adsorption of rSPG by the IgG@Fe_3O_4-PEI composite. However, for BSA, IgG modification had minimal impact on adsorption efficiency, indicating that its adsorption primarily resulted from the non-specific interaction with Fe_3O_4-PEI. For Lys, IgG modification effectively minimized non-specific adsorption, thus confirming the exceptional selectivity of the IgG@Fe_3O_4-PEI composite for rSPG.

The effect of the ionic strength on the protein adsorption efficiency was studied at pH 6.0. As shown in Fig. 3C the adsorption efficiency of the IgG@Fe_3O_4-PEI composite for rSPG and BSA decreased as the neutral salt concentration increased from 0 to 500 mmol L^{-1}. The observed reduction occurred due to ion competition, which decreased the protein-composite interactions and subsequently lowered adsorption efficiency. Since high ionic strength hinders protein adsorption, the pH 6.0 BR buffer was selected as the optimal experimental condition.

Fig. 4A shows the influence of the adsorption time on the adsorption efficiency of rSPG by IgG@Fe_3O_4-PEI composite. In the adsorption time range of 0–75 min, the adsorption efficiency of rSPG on the IgG@Fe_3O_4-PEI composite gradually increased, reaching its maximum at 60 min before stabilizing at equilibrium. The adsorption time data were fitted to pseudo-first-order, pseudo-second-order, intraparticle diffusion, and Elovich kinetic models, with the relevant parameters presented in Figs. S1-S2. The adherence of the adsorption process to each model was determined based on data fitting results and correlation coefficients. The non-linear pseudo-second-order kinetic model ($R^2 = 0.9678$) provided the best fit, indicating that chemical adsorption is the dominant mechanism.

Fig. 4B shows the effect of adsorption temperature on rSPG. As shown in Fig. 4B, the adsorption efficiency of the IgG@Fe_3O_4-PEI composite for rSPG increased with temperature but decreased beyond a certain point within the 5–60 °C range. The observed behavior was attributed to the reduced chemical reaction rate at lower temperatures, decreasing the protein-adsorbent interactions. Thus, at low temperatures, the decreased reaction rate limits protein-adsorbent interactions, therefore decreasing adsorption efficiency. At high temperatures, conformational changes in the protein may alter its binding sites, hindering its interaction with the adsorbent surface [47]. The described structural alteration can decrease the protein-adsorbent interactions, reducing adsorption efficiency. Therefore, the optimal adsorption conditions were identified as 1 h and 25 °C.

To evaluate the adsorption capacity of the IgG@Fe_3O_4-PEI composite for rSPG, its adsorption ability was examined at pH 6.0 across varying rSPG concentrations (100–1,200 μg·mL^{-1}) and the observed results are shown in Fig. S3. With an increase in the concentration, the unit adsorption capacity of the IgG@Fe_3O_4-PEI composite progressively increased. However, once the concentration exceeded 1000 μg·mL^{-1}, the adsorption capacity remained constant, suggesting that the adsorption sites were approaching saturation condition. The adsorption capacity was measured under various conditions and analyzed using Langmuir, Freundlich, and Dubinin-Radushkevich adsorption isotherm models, as shown in Fig. S3. The experimental data aligned well with the Langmuir model ($R^2 = 0.993$). The theoretical maximum adsorption capacity was calculated to be 125.0 mg·g^{-1} using the intercept of the linear equation.

The desorption efficiency of various eluents was examined to optimize rSPG elution from the IgG@Fe_3O_4-PEI composite. The investigated eluents included BR buffers at pH 10.0 and pH 4.0, deionized water, and PBS (0.01 mol L^{-1}, pH 7.2). As presented in Fig. 5A, BR (pH 10.0) achieved a recovery rate of 95.81 % for rSPG, whereas the other three eluents demonstrated low recovery efficiency. At pH 10.0, enhanced electrostatic repulsion decreased the interaction between rSPG and the material surface, thus facilitating its desorption and recovery. The

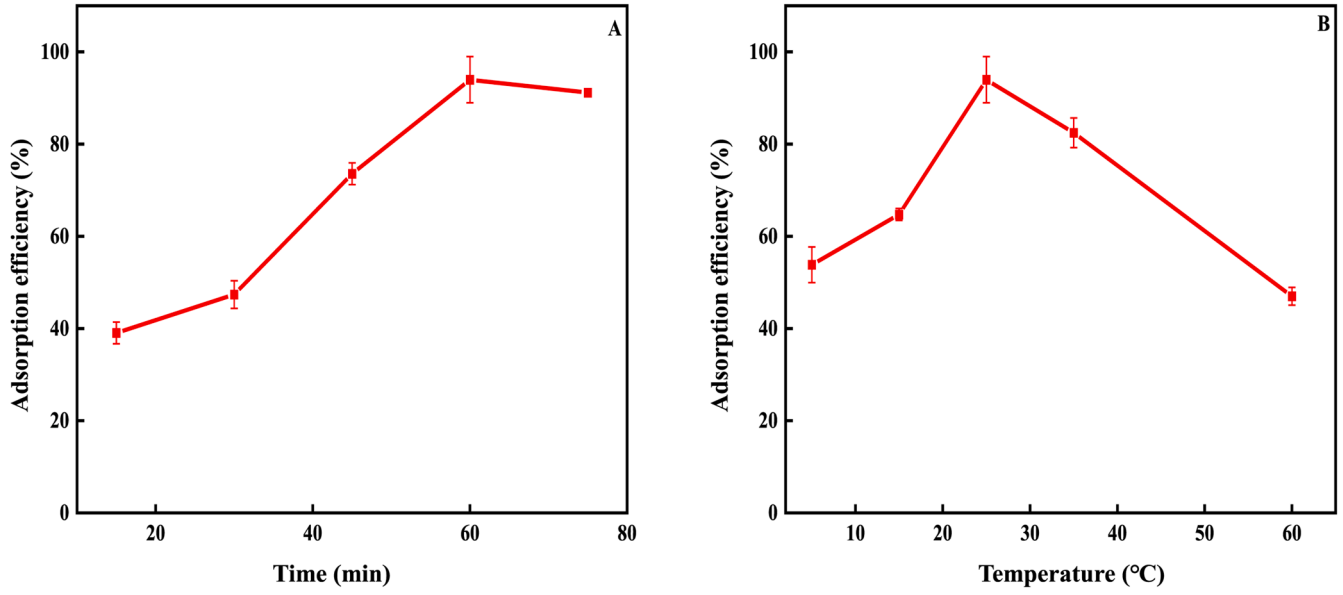

Fig. 4. Effect of the adsorption time (A) and adsorption temperature (B) on adsorption efficiency of rSPG. Protein solution: 100 μg mL^{-1}, 100 μL; IgG@Fe_3O_4-PEI: 0.5 mg.

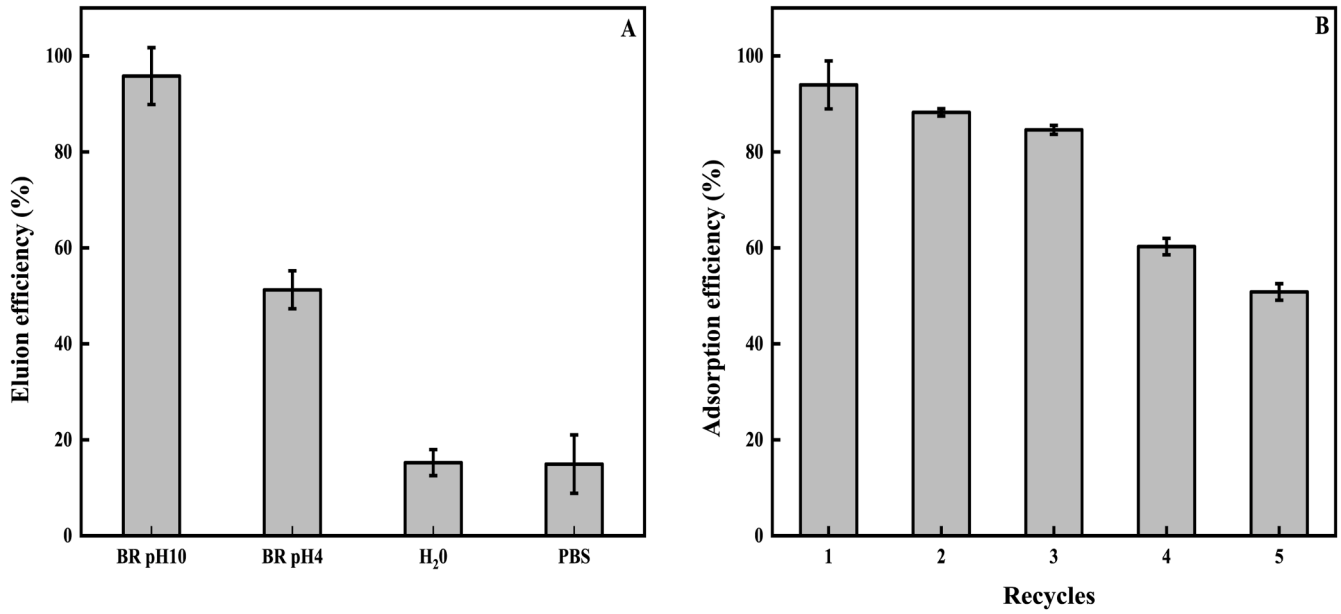

Fig. 5. Recovery of adsorbed rSPG from the IgG@Fe_3O_4-PEI composite using various elution. Reproducibility of the rSPG adsorption performance of the IgG@Fe_3O_4-PEI composite (B). Protein solution: 100 μg mL^{-1}100 μg mL^{-1}; IgG@Fe_3O_4-PEI: 0.5 mg; Elution agent: 100 μL.

durability of the IgG@ Fe_3O_4-PEI composite was investigated by evaluating its ability to retain high adsorption efficiency for rSPG over multiple adsorption-desorption cycles. The result presented in Fig. 5B indicated that the adsorption efficiency of rSPG by IgG@Fe_3O_4-PEI composite remained stable at approximately 80 % after 3 cycles. After three cycles, the adsorption efficiency gradually declined, indicating a limitation in long-term reuse. However, the IgG@ Fe_3O_4-PEI composite demonstrated a promising potential for repeated applications in rSPG purification.

The adsorption and elution processes can affect the secondary structure of the protein, hence potentially influencing its stability and functionality in further research. Circular dichroism (CD) analysis was performed to assess whether the rSPG recovered from the IgG@ Fe_3O_4-PEI composite experienced denaturation. This method was used to evaluate conformational changes in rSPG, with BR (pH 10.0) buffer serving as the elution agent (Fig. 6). Fig. 6a presents the CD spectrum of the rSPG standard solution in water, where a negative peak at 214 nm indicates the presence of α-helix structures in the protein [48]. Similarly, Fig. 6b displays the CD spectrum of rSPG eluted using BR (pH 10.0) buffer, demonstrating a peak consistent with the water-soluble rSPG standard, suggesting that the protein's secondary structure remained intact. These findings suggested that the adsorption and elution process of rSPG on the surface of the IgG@Fe_3O_4-PEI composite did not affect its structure.

3.3. Separation of rSPG from protein mixture samples

rSPG is typically produced on a large scale by introducing the target gene into an *E. coli* expression system [49]. Since Lys is commonly present in *E. coli*, mixed samples of rSPG and Lys were used in this experiment to further assess the enrichment capability of the composite material for rSPG. In Fig. 7, lane 2 shows the mixed protein solution

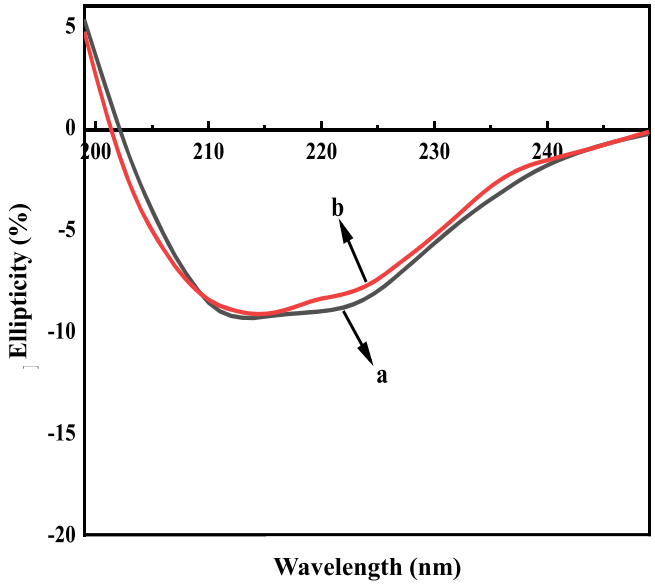

Fig. 6. CD spectra of rSPG: 100 μg mL^{-1} rSPG in deionized water and (a); rSPG eluted into the BR (pH 10.0) buffer (b).

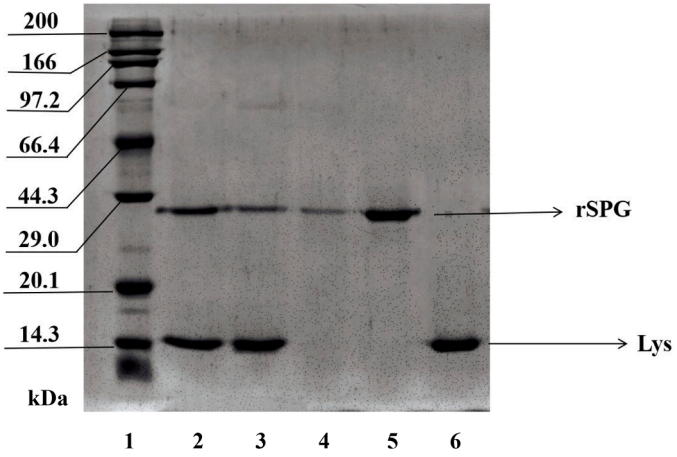

Fig. 7. SDS-PAGE analysis of protein adsorption and recovery. Lane 1: molecular weight standards; Lane 2: A mixture of rSPG and Lys protein solution; Lane 3: Supernatant of the rSPG and Lys mixed protein solution after adsorption with IgG@Fe_3O_4-PEI composite; Lane 4: rSPG recovered after elution with BR (pH 10.0) buffer; Lane 5: rSPG standard solution; Lane 6: Lys standard solution.

containing rSPG (28 kDa) and Lys (14.4 kDa), while lane 3 displays the supernatant after adsorption by the IgG@ Fe_3O_4-PEI composite. The band corresponding to rSPG became lighter compared to that before the adsorption, whereas the band corresponding to Lys remained unchanged. Lane 4 shows the supernatant of the IgG@Fe_3O_4-PEI composite after elution with BR (pH 10.0) buffer, showing a distinct band at 28 kDa, which aligned with the standard rSPG band in lane 5. This finding confirmed that the composite was capable of effectively separating and enriching rSPG from mixed protein samples.

3.4. Separation of rSPG from complex biological samples

E. coli can be used as a complex biological sample to evaluate the anti-interference ability of materials. To evaluate the practicality of the IgG@ Fe_3O_4-PEI composite, an *E. coli* lysate was mixed with rSPG as a complex matrix. In Fig. 8A, lane 2 represents the *E. coli* lysate without added protein, lane 3 represents the *E. coli* lysate with added rSPG, and lane 4 represents the supernatant of the *E. coli* lysate after the adsorption by IgG@Fe_3O_4-PEI composite. The protein band corresponding to rSPG became lighter, hence indicating adsorption, while the band observed after elution with BR (pH 10.0) buffer (lane 5) aligned with the standard rSPG position (lane 6), thus confirming successful separation and recovery. The described electrophoresis result demonstrated that the IgG@Fe_3O_4-PEI composite can separate and enrich rSPG from complex matrices.

Moreover, the IgG@Fe_3O_4-PEI composite was applied for the separation and purification of rSPG in the *E. coli* expression system. Fig. 8B shows the SDS-PAGE analysis results, where lane 2 and lane 3 corresponded to the *E. coli* lysate without and with the inducer, respectively. A dense protein band was observed at the 31 kDa in lane 3, indicating the successful recombinant expression of rSPG. The *E. coli* lysate containing successfully expressed rSPG was adsorbed by the IgG@Fe_3O_4-PEI composite, resulting in a lighter protein band at the rSPG position in lane 4. After elution and recovery, lane 5 displayed a distinct band aligning with the rSPG position, confirming that the IgG@Fe_3O_4-PEI composite effectively enriched rSPG from the expression system of *E. coli*.

3.5. Extraction of low-abundance proteins from serum samples

The protein was extracted from the serum samples using the IgG@Fe_3O_4-PEI complex. The extracted protein was subsequently analyzed using mass spectrometry and data-independent acquisition (DIA) techniques. A total of 430 proteins were identified, 34 of which were undetectable in untreated serum samples, highlighting the effectiveness of the method in trapping low-abundance proteins Fig. 9D The first 17 proteins of each sample were analyzed. The results showed that treatment with IgG@Fe_3O_4-PEI enriched low-abundance proteins, such as plasma protease C1 inhibitor, immunoglobulin J chain, alpha-1-antichymotrypsin and ceruloplasmin, CD5 antigen-like, kininogen-1, alpha-2-glycoprotein, vitamin D-binding protein, transthyretin, and others (Fig. 9A-C). These proteins have potential interactions with IgG, however, the interaction between alpha-1-antichymotrypsin and IgG is not well studied. Therefore, Alphafold3 was used to predict the molecular interactions of IgG heavy chain and alpha-1-antichymotrypsin, showing the results of ipTM=0.63 and pTM=0.53, with high confidence. The protein docking structure demonstrates the potential binding force of its presence (Scheme 2). The IgG molecule is composed of four polypeptide chains, two heavy chains (H chains) and two light chains (L chains), which are connected by disulfide bonds to form a Y-shaped structure. Each heavy chain contains a constant region (Fc region) and a variable region (Fab region). The Fc region is located in the "tail" of the antibody and consists of constant regions of two heavy chains. The Fc region plays a key role in the biological effects of IgG, such as binding to

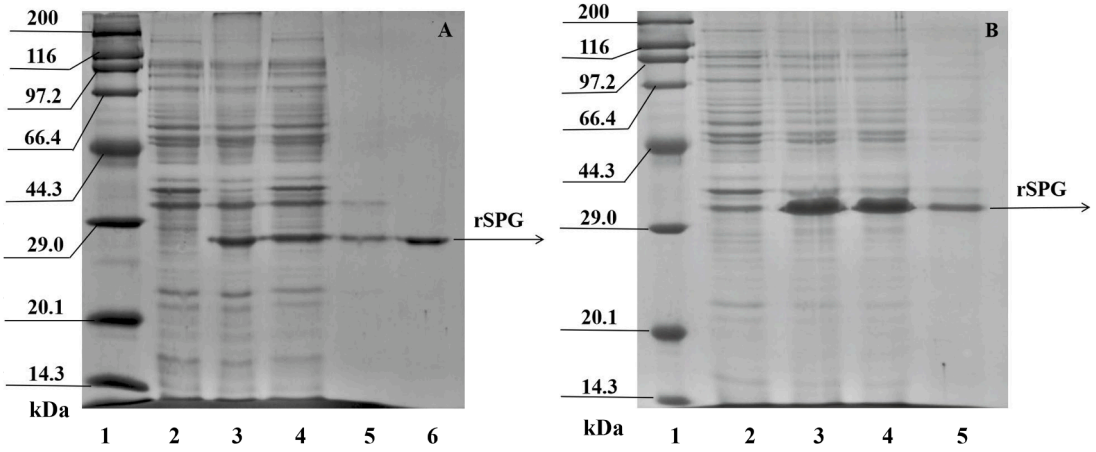

Fig. 8. SDS-PAGE analysis of rSPG adsorption from *E. coli* lysate (A). Lane 1: molecular weight standards; Lane 2: unlabeled lysate of *E. coli*. Lane 3: lysate of *E. coli* with added rSPG; Lane 4: supernatant of labeled lysate of *E. coli* after the adsorption of rSPG with IgG@Fe_3O_4-PEI composite. Lane 5: rSPG recovered after elution with the BR (pH 10.0) buffer; Lane 6: rSPG standard solution. Adsorption of rSPG from the *E. coli* expression system (B). Lane 1: molecular weight standards; Lane 2: uninduced lysate of *E. coli* without the IPTG inducer. Lane 3: induced lysate of *E. coli* with the IPTG inducer. Lane 4: lysate of *E. coli* after adsorption with the IgG@Fe_3O_4-PEI composite. Lane 5: rSPG recovered after elution with the BR (pH 10.0) buffer.

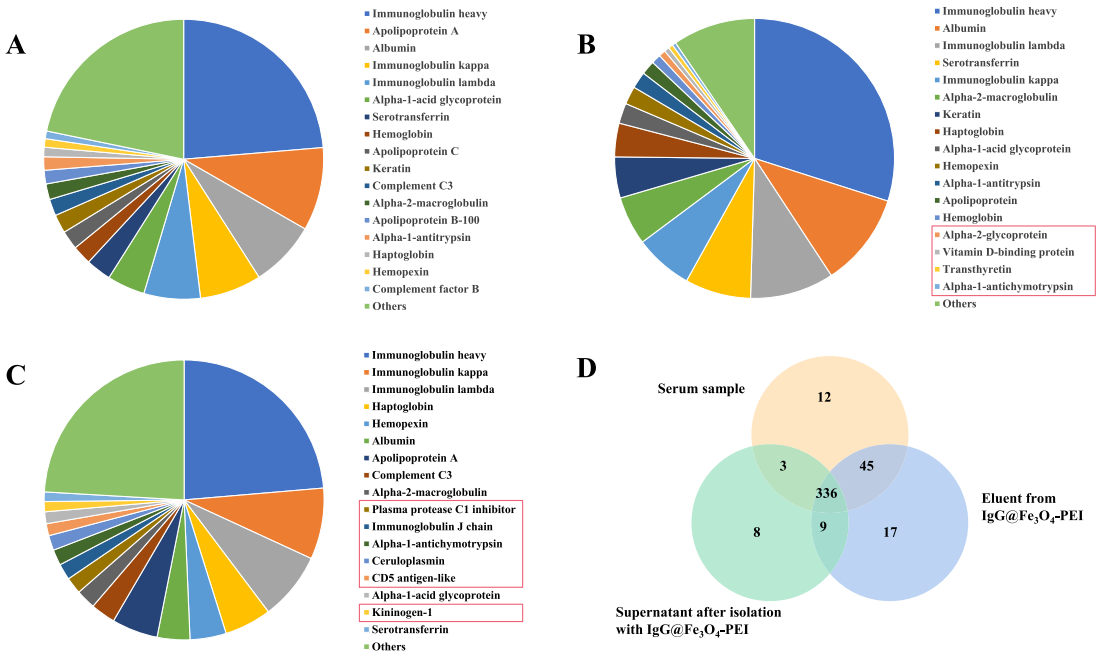

Fig. 9. Distribution of the top eleven proteins in serum (A). Protein distribution of the top eleven remaining contents in the supernatant after adsorption (B) Elution from the material under the content of the top eleven protein distributions (C) Venn diagram of the distribution of protein species in human serum, supernatant after adsorption, and elution from the material (D).

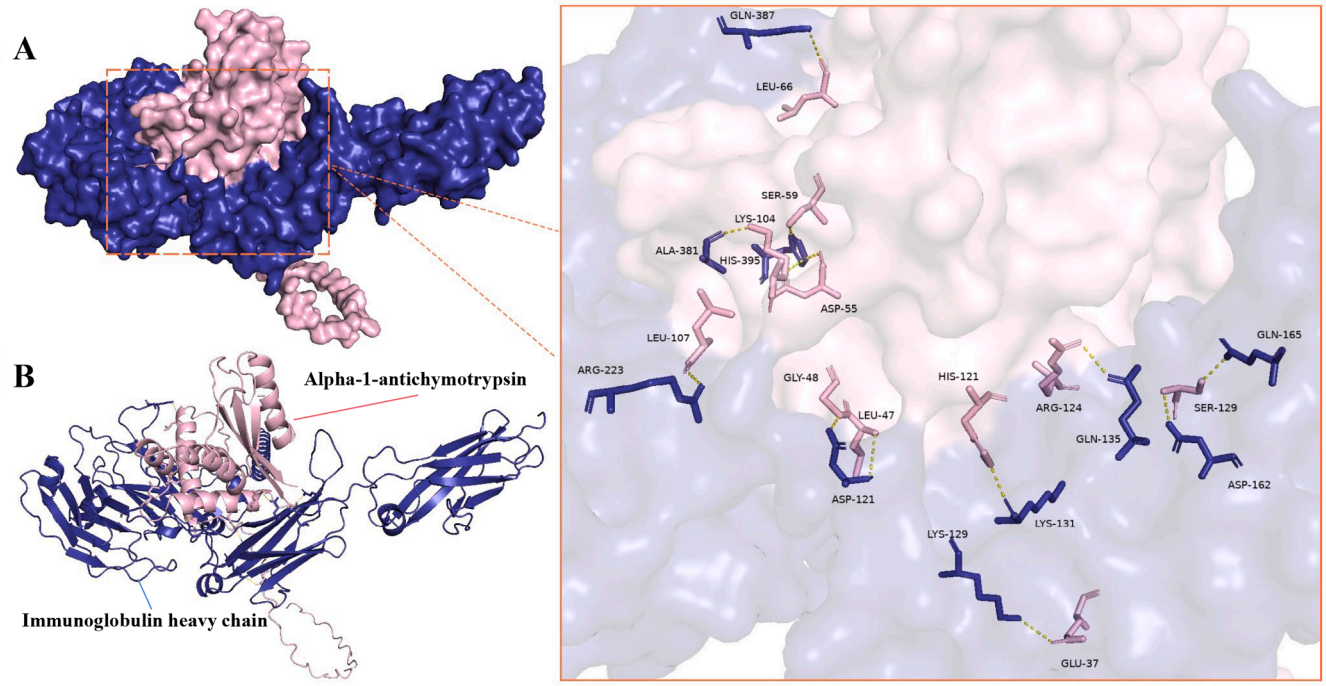

Scheme 2. Protein molecular docking analysis of immunoglobulin with alpha-1-antichymotrypsin.

immune cell receptors. The Fc region of IgG binds to a variety of Fc receptors on the surface of immune cells, such as FcγR. Through this binding, IgG can activate immune effects such as phagocytosis and antibody-dependent cell-mediated cytotoxicity (ADCC) [50]. Alpha-1-antichymotrypsin plays an important role in inflammation, infection, and tissue repair, such as rheumatoid arthritis [51], inflammatory bowel disease [52], etc. Therefore, studying the interaction between alpha-1-antichymotrypsin and IgG in immune regulation and inflammatory response will give new insights into disease prevention. The specific adsorption strategy of IgG@Fe_3O_4-PEI was thus applied to rSPG for identifying low-abundance proteins in human serum samples, leading to the discovery of protein-protein interactions, and providing research ideas for the diagnosis, treatment, and prevention of diseases.

4. Conclusions

In this study, magnetic nanoparticles were successfully modified with IgG to fabricate the IgG@Fe_3O_4-PEI composite. The characterization results demonstrated that the IgG@Fe_3O_4-PEI composite effectively separated and purified rSPG under optimal conditions. Furthermore, mass spectrometry and molecular docking analyses revealed a novel interaction between IgG and a previously unidentified protein. This finding, along with molecular docking results, suggested that the Fc fragment of IgG played a key role in the interaction, providing new insights into the Fc-mediated binding mechanisms. These findings pave the way for targeted protein analysis in complex biological systems. Overall, the IgG@Fe_3O_4-PEI composite provides significant potential for proteomics research and clinical applications, particularly in isolating and identifying low-abundance proteins.

Ethical approval

This study was reviewed and approved by Ethics Committee of Shenyang Medical College (2024 Ethics Review No. 4).

CRediT authorship contribution statement

Dajun Zhang: Writing – original draft, Investigation, Funding acquisition, Formal analysis, Data curation. **Yufei Ma:** Writing – original draft, Investigation, Formal analysis, Data curation, Conceptualization. **Ying Wang:** Software, Investigation, Conceptualization. **Xiangyu Liu:** Visualization, Software, Conceptualization. **Mengfan Zhao:** Visualization, Software, Resources, Methodology. **Yuanke Wang:** Validation, Resources. **Song Gao:** Validation, Supervision, Project administration. **Fu Ren:** Writing – review & editing, Resources, Investigation, Funding acquisition. **Qing Chen:** Writing – review & editing, Writing – original draft, Software, Resources, Project administration, Investigation, Funding acquisition, Formal analysis, Data curation.

Declaration of competing interest

The authors declare that they have no known competing financial interests or personal relationships that could have appeared to influence the work reported in this paper.

Acknowledgments

The authors gratefully acknowledge the financial support from the following funding agencies: the National Natural Science Foundation of China (Grant No. 21804093), the Key R&D Project of the Liaoning Provincial Department of Science and Technology (Grant No. 2025JH2/102800051), the Future Industry Frontier Technology Project of the Liaoning Provincial Department of Science and Technology (Grant No. 2025080219-JH2/1013), the Project of the Science and Technology Department of Liaoning Province (Grant No. 2024-MS-226), the Self-Developed Research Project of the Education Department of Liaoning Province (Grant No. JYTMS20231407), the Shenyang Young and Middle-aged Science and Technology Innovation Talent Project (Grant No. RC230168), and the Liaoning Province Key Laboratory for Phenomics of Human Ethnic Specificity and Critical Illness (Grant No. [2022]59).The authors thank the Shanghai Luming biological technology co., LTD (Shanghai, China) for providing proteomics services and all the reviewers who participated in the review and MJEditor (www.mjeditor.com) for its linguistic assistance during the preparation of this manuscript.

Supplementary materials

Supplementary material associated with this article can be found, in the online version, at doi:10.1016/j.surfin.2025.107622.

Data availability

No data was used for the research described in the article.

References

[1] T.E. Mulroney, T. Pöyry, J.C. Yam-Puc, et al., N1-methylpseudouridylation of mRNA causes +1 ribosomal frameshifting, Nature 625 (2024) 189–194.
[2] J. Mahlangu, R. Kaczmarek, A. von Drygalski, et al., GENEr8-1 Trial group, two-year outcomes of Valoctocogene Roxaparvovec therapy for hemophilia A, N. Engl. J. Med. 388 (2023) 694–705.
[3] M. Korodi, K. Rákosi, M. Baibarac, et al., Reusable on-plate immunoprecipitation method with covalently immobilized antibodies on a protein G covered microtiter plate, J. Immunol. Methods 483 (2020) 112812.
[4] D. Kim, K. Karns, S.Q. Tia, et al., Electrostatic protein immobilization using charged polyacrylamide gels and cationic detergent microfluidic western blotting, Anal. Chem. 84 (2012) 2533–2540.
[5] J.S. Lin, E.M. Lai, Protein-protein interactions: co-immunoprecipitation, Methods Mol. Biol. 1615 (2017) 211–219.
[6] S.J. Song, H.P. Diao, B. Moon, et al., The B1 domain of streptococcal protein G serves as a multi-functional tag for recombinant protein production in plants, Front. Plant Sci. 13 (2022) 878677.
[7] S.G. Kim, J.Y. Kim, M.Y. Kim, et al., Autodisplay of streptococcal protein G for construction of an orientation-controlled immunoaffinity layer, Analyst 148 (2023) 742.
[8] H. Zhang, W. Liang, H. Fan, et al., Immunological characterization and verification of recombinant streptococcal protein G, Mol. Med. Rep. 12 (2015) 6311–6315.
[9] Q. Zhuang, A. Shen, L. Liu, et al., Prognostic and immunological roles of Fc fragment of IgG binding protein in colorectal cancer, Oncol. Lett. 22 (2021) 526.
[10] C. Yang, B. He, H. Zhang, et al., IgG Fc affinity ligands and their applications in antibody-involved drug delivery: a brief review, Pharmaceutics. 15 (2023) 187.
[11] E. Chalayer, B. Gramont, F. Zekre, et al., Fc receptors gone wrong: a comprehensive review of their roles in autoimmune and inflammatory diseases, Autoimmun. Rev. 21 (2022) 103016.
[12] E.C. So, H. Zhou, A. Greenwell, et al., Complement component C1q is an immunological rheostat that regulates fc:fc[Formula: see text]R interactions, Immunogenetics 75 (2023) 369–383.
[13] J. Liu, R. Shen, L. Feng, et al., Proteomics study of Mycoplasma pneumoniae pneumonia reveals the Fc fragment of the IgG-binding protein as a serum biomarker and implicates potential therapeutic targets, Front. Med. 16 (2022) 378–388.
[14] E.A. Fitzpatrick, J. Wang, S.E. Strome, Engineering of Fc Multimers as a protein therapy for autoimmune disease, Front. Immunol. 11 (2020) 496.
[15] G.S. El-Sayyad, O.F. Hasan, M.A.M. Saad, et al., Improving the diagnosis of bovine tuberculosis using gold nanoparticles conjugated with purified protein derivative: special regard to staphylococcal protein A and streptococcal protein G, Environ. Sci. Pollut. Res. Int. 28 (2021) 29200–29220.
[16] D. Wang, X. Chen, J. Feng, M. Sun, Recent advances of ordered mesoporous silica materials for solid-phase extraction, J. Chromatogr. A 1675 (2022) 463157.
[17] Z. Wang, C. Zhang, J. Meng, et al., A targeted exosome therapeutic confers both cfDNA acavenging and macrophage polarization for ameliorating rheumatoid arthritis, Adv. Mater. (2023) 2302503.
[18] F. Augusto, L.W. Hantao, N.G.S. Mogollón, et al., New materials and trends in sorbents for solid-phase extraction, Trends Anal. Chem. 43 (2013) 14–23.
[19] H.D. Li, Y.Q. Chen, Y. Li, et al., Harnessing virus flexibility to selectively capture and profile rare circulating target cells for precise cancer subtyping, Nat. Commun. 15 (2024) 5849.
[20] M.J. Archer, B. Lin, Z. Wang, et al., Magnetic bead-based solid phase for selective extraction of genomic DNA, Anal. Biochem. 355 (2006) 285–297.
[21] I.M.M. Rahman, Z.A. Begum, H. Hasegawa, Selective separation of elements from complex solution matrix with molecular recognition plus macrocycles attached to a solid-phase: a review, Microchem. J. 110 (2013) 485–493.
[22] D. Sun, M. Chen, X. Zhang, et al., Separation of hydrogen isotopic water by multi-walled carbon nanotube (MWCNT) membrane and graphene oxide (GO)-MWCNT composite membranes, Sep. Purif. Technol. 344 (2024) 127275.
[23] M. Pastucha, Z. Farka, K. Lacina, et al., Magnetic nanoparticles for smart electrochemical immunoassays: a review on recent developments, Mikrochim. Acta 186 (2019) 312.
[24] D.Y. Kang, J.S. Lee, Challenges in developing MOF-based membranes for gas separation, Langmuir. 39 (2023) 2871–2880.
[25] J. Zhong, Y. Cao, J. Zhu, et al., Facile construction of phenolic hydroxyl anchored covalent organic frameworks/chitosan composite aerogels for efficient adsorption of Pb (II) from water, Separation and Purification Technology, Sep. Purif. Technol. 354 (2025) 129087.
[26] Y. Zhang, D.D. Zhang, X. Wu, et al., A novel Anderson-Evans polyoxometalate-based metal-organic framework composite for the highly selective isolation and purification of cytochrome c from porcine heart, Colloids. Surf. B: Biointerfaces. 213 (2022) 112420.
[27] Q. Li, H. Chen, X. Feng, et al., Nanoparticle-regulated semiartificial magnetotactic bacteria with tunable magnetic moment and magnetic sensitivity, Small. 15 (2019) 1900427.
[28] Wang M.M., Chen Q., Zhang D.D., et al., Tetra-nickel substituted polyoxotungsate as an efficient sorbent for the isolation of His6-tagged proteins from cell lysate, Talanta, 17, 173–178.

[29] F. Mollarasouli, E. Zor, G. Ozcelikay, et al., Magnetic nanoparticles in developing electrochemical sensors for pharmaceutical and biomedical applications, Talanta 226 (2021) 122108.
[30] E. Öztürk Er, G. Dalgıç Bozyiğit, Ç. Büyükpınar, S. Bakırdere, Magnetic nanoparticles based solid phase extraction methods for the determination of trace elements, Crit. Rev. Anal. Chem. 52 (2020) 231–249.
[31] X. Yao, R. Xie, Y. Cao, et al., Simvastatin induced ferroptosis for triple-negative breast cancer therapy, J. Nanobiotechnol. 19 (2021) 311.
[32] Z. Shen, T. Liu, Y. Li, et al., Fenton-reaction-acceleratable magnetic nanoparticles for ferroptosis therapy of orthotopic brain tumors, ACS. Nano 12 (2018) 11355–11365.
[33] R. Taghavi, S. Rostamnia, M. Farajzadeh, et al., Magnetite metal-organic frameworks: applications in environmental remediation of heavy metals, organic contaminants, and other pollutants, Inorg. Chem. 61 (2022) 15747–15783.
[34] S. Narimani-Sabegh, E. Noroozian, Magnetic solid-phase extraction and determination of ultra-trace amounts of antimony in aqueous solutions using maghemite nanoparticles, Food Chem. 287 (2019) 382–389.
[35] X. Zhu, L. Zhang, A. Fu, et al., Efficient purification of lysozyme from egg white by 2-mercapto-5-benzimidazolesulfonic acid modified Fe_3O_4/Au nanoparticles, Mater. Sci. Eng. C. Mater. Biol. Appl. 59 (2016) 213–217.
[36] S. Sun, M. Ma, N. Qiu, et al., Affinity adsorption and separation behaviors of avidin on biofunctional magnetic nanoparticles binding to iminobiotin, Colloids. Surf. B: Biointerfaces. 88 (2011) 246–253.
[37] U.K. Laemmli, Cleavage of structural proteins during the assembly of the head of bacteriophage T4, Nature 227 (1970) 680–681.
[38] P. Pandey, G. Pandey, R. Narayan, Polyethylenimine-mediated controlled synthesis of Prussian blue-gold nanohybrids for biomedical applications, J. Biomater. Appl. 36 (2021) 26–35.
[39] J.L. Zhang, R.S. Srivastava, R.D. Misra, Core-shell magnetite nanoparticles surface encapsulated with smart stimuli-responsive polymer: synthesis, characterization, and LCST of viable drug-targeting delivery system, Langmuir. 23 (2007) 6342–6351.
[40] T. Wang, X. Hu, Y. Yang, et al., New insight into assembled Fe_3O_4@PEI@Ag structure as acceptable agent with enzymatic and photothermal properties, Int. J. Mol. Sci. 23 (2022) 10743.
[41] A. Barth, C. Zscherp, What vibrations tell us about proteins, Q. Rev. Biophys. 35 (2002) 369–430.
[42] Y. Zhen, L. Chen, X.Y. Ma, et al., Amyloid peptide 1-42-conjugated magnetic nanoparticles for the isolation and purification of glycoproteins in Egg White, ACS. Appl. Mater. Interfaces. 13 (2021) 14028–14036.
[43] M. Kluz-Barłowska, T. Kluz, W. Paja, et al., FT-Raman data analyzed by multivariate and machine learning as a new method for detection spectroscopy marker of platinum-resistant women suffering from ovarian cancer, Sci. Rep. 13 (2023) 20772.
[44] H.G. Lee, S. Kang, J.S. Lee, Binding characteristics of staphylococcal protein A and streptococcal protein G for fragment crystallizable portion of human immunoglobulin G, Comput. Struct. Biotechnol. J. 19 (2021) 3372–3383.
[45] R.K. Jha, T. Gaiotto, A.R. Bradbury, et al., An improved protein G with higher affinity for human/rabbit IgG fc domains exploiting a computationally designed polar network, Protein Eng. Des. Sel. 27 (2014) 127–134.
[46] T. Yokoyama, M. Mizuguchi, Y. Nabeshima, et al., Hydrogen-bond network and pH sensitivity in human transthyretin, J. Synchrotron. Radiat. 20 (2013) 834–837.
[47] M. Dong, A minireview on temperature dependent protein conformational sampling, Protein J. 40 (2021) 545–553.
[48] W.C. Pomerantz, T.L. Grygiel, J.R. Lai, S.H. Gellman, Distinctive circular dichroism signature for 14-helix-bundle formation by beta-peptides, Org. Lett. 10 (2008) 1799–1802.
[49] H. Zhang, W. Liang, H. Fan, et al., Immunological characterization and verification of recombinant streptococcal protein G, Mol. Med. Rep. 12 (2015) 6311–6315.
[50] D. Četić, G. Miljuš, Z. Dobrijević, et al., Simultaneous isolation and purification of transferrin and immunoglobulin G from Human serum-A new biotech solution, Molecules. 21 (2025) 993.
[51] M.D. Chard, J. Calvin, C.P. Price, T.E. Cawston, B.L. Hazleman, Serum alpha 1 antichymotrypsin concentration as a marker of disease activity in rheumatoid arthritis, Ann. Rheum. Dis. 47 (1988) 665–671.
[52] E.J. Hollox, β-defensins and Crohn's Disease: confusion from counting copies, Am. J. Gastroenterol. 105 (2010) 360–362.